This is the submitted version of the article: Contreras, AR. et al. *Cerium oxide nanoparticles anchored onto graphene oxide for the removal of heavy metal ions dissolved in water* in Desalination and water treatment (Taylor and Francis ed.), vol. 214 (2018), p. 134-145.

DOI 10.5004/dwt.2018.22735

Cerium oxide nanoparticles anchored onto graphene oxide for the removal of heavy metal ions dissolved in water

Ada Rebeca Contreras Rodríguez,[a] Joseph E. McCarthy,[b] Amanda Alonso,[a,] Xavier Font,[a] Yurii K. Gun'ko[b,c] and Antoni Sánchez[a*]*

a.Department of Chemical, Biological and Environmental Engineering, Escola d'Enginyeria, Universitat Autònoma de Barcelona, 08193 Bellaterra, Spain.

b.School of Chemistry, Trinity College Dublin, Dublin 2, Ireland

c.ITMO University, 197101 Saint Petersburg, Russia.

Dra. Ada Rebeca Contreras Rodríguez. E-mail: adarebecac@gmail.com. Dr. Joseph E. McCarthy. Phone: +35386088682. E-mail: mccartj5@tcd.ie. Dra. Amanda Alonso. Phone: +34935811018. E-mail: Amanda.alonso@uab.cat. Dr. Yurii K. Gun'ko. Phone: +35318963543. E-mail: igounko@tcd.ie. Dr. Xavier Font. Phone: +34935814480. E-mail: Xavier.font@uab.cat

Corresponding Author:

* Dr. Antoni Sánchez. Phone: +34-935814793. Fax: +34-935812013. E-mail: Antoni.sanchez@uab.cat

ABSTRACT

The aim of this study is to investigate the possibility of using Cerium Oxide (CeO_2) nanoparticles (NPs) attached to reduced graphene oxide (rGO) as an alternative adsorbent for cadmium (II), lead (II) and chromium (VI) removal from aqueous solution. The new nanomaterials (CeO_2/rGO) were obtained following two different strategies, in-situ growth and self-assembly approach. The adsorption capacities for each heavy metal were investigated at a fixed pH (5.5-6), a range concentration of heavy metal from 5 to 250 mg/L and a fixed concentration of 0.05 mg of CeO_2/rGO nanomaterial. The experimental data were fitted using the Langmuir, Freundlich and Temkin isotherms models. The experimental data of each nanomaterial for the removal of Pb(II) were approximated best by the Langmuir model, while for the removal of Cd(II) Langmuir and Freundlich showed good regression coefficients. The study showed that CeO_2 NPs attached to rGO could be used as an efficient adsorbent material for the adsorption of cadmium and lead from aqueous solution. The nanomaterial obtained by *in-situ* growth registered the highest adsorption capacity for the removal of lead (95.75 mg Pb^{2+}/g CeO_2/rGO-HMT), meanwhile in the case of cadmium the highest adsorption was obtained with the nanomaterial synthesized following the self-assembly approach (31.26 mg Cd^{2+}/ g CeO_2/rGO-AM).

KEYWORDS

Cerium oxide nanoparticles; in-situ growth; self-assembly; Graphene oxide; Heavy metals removal; nanocomposite.

1. Introduction

Cerium oxide (CeO_2) is a rare earth oxide with a wide range of applications in catalysis, UV-blocking and oxygen sensors [1]. In addition, some studies used CeO_2 nanoparticles (NPs) as suitable adsorbent for the elimination of heavy metal ions [2–4]. Graphene and graphene oxide (GO) have been the hotspot in multidisciplinary areas due to its excellent mechanical, thermal, and electrical properties. In addition, both graphene and GO can be doped with metal oxides resulting in nanomaterials that usually have features that make them suitable materials for the effective sequestration of heavy metal ions due to their excellent adsorption performance [5,6]. Moreover, in the case of organic pollutants or persistent organic pollutants, those nanomaterials decompose the pollutants to less toxic molecules [7].

One of the biggest limiting steps in the application of graphene-based nanomaterials in environmental fields is the agglomeration of the graphene sheets to form graphite due to Van der Waals interactions. To overcome this drawback, a growing exploration to modify (due to the presence of oxygen containing functional groups on their surface), immobilize or anchor NPs or other materials onto graphene has been tested [8]. Different approaches have been studied for the synthesis of hybrids nanomaterials based on graphene and metal NPs [9–11]. Recent studies suggest that reduced graphene oxide (rGO) and GO supported materials have higher binding capacity compared to free NPs [12]. Additionally, another aspect to take into account for using such composites for application in environmental remediation, such as water purification, is the ease of solid–liquid separation and post treatment-handling [12–14].

In this study, two different strategies to obtain a hybrid material composed of CeO_2 NPs anchored to the surface of GO: *self-assembly* approach and *in-situ* growth, followed by a

63 chemical reduction of the GO becoming CeO_2/rGO, in both cases. The *self-assembly* approach is
64 based in a two-step synthesis, in which the first step is to synthesize the NPs with specific
65 dimensions and morphologies using different stabilizers, such as 6-aminohexanoic acid (AHA)
66 [1] or hexamethylenetetramine (HMT) [15], followed by the attachment of the NPs on the
67 surface of the GO in a second step. On the other hand, the *in-situ* growth suggests the growth of
68 NPs directly in the basal planes of the graphene oxide [1]. In most hybrid materials, the metal
69 NPs deposited on graphene often exhibit easily agglomeration under the high temperature used
70 in the synthesis. Many studies suggest the addition of organic additives such as acrylamide (AM)
71 [16] or poly(vinylpyrrolidone) (PVP) [1] to control the NPs dispersion and size.

72 In this work, the *in-situ* strategy is based on the electrostatic adsorption of positively charged
73 Ce^{3+} ions on the basal planes of GO sheets, that are highly negatively charged when dispersed in
74 water [17], followed by in situ growth of CeO_2 on GO sheets, and finally the conversion of GO
75 into rGO. On the other hand, the *self-assembly* strategies go through the direct deposition of
76 CeO_2 NPs on the surface of the GO sheets followed by the reduction of GO to rGO [1,16].

77 According to Ji et al.[1] during the *self-assembly* process of the CeO_2/rGO-AHA nanomaterial,
78 the AHA-stabilized CeO_2 were prepared as a first step, in which the carboxylic acid of the AHA
79 binds to the surface of the CeO_2 NPs and releases a proton to form a carboxylate group. The
80 proton then protonates the amino group of AHA, generating a positively charged surface for the
81 CeO_2 NPs [18]. As mentioned before, the assembly of the CeO_2 NPs (stabilized with AHA) on
82 the GO sheets is provided by the electrostatic interactions between the surface of the NPs and the
83 surface of the GO, creating a well combined nanocomposite [1].

The objective of this study was to investigate the influence of these two strategies in the distribution and size of the NPs and thus, in their properties as adsorbents. Furthermore, the adsorption capacity for cadmium (II), lead (II) and chromium (VI) ions onto the new nanomaterials synthetized was tested and fitted using Langmuir, Freundlich and Temkin isotherm adsorption models. To the best of our knowledge, this is the first study where GO derived materials are effectively used for the removal of highly toxic heavy metals in a wide range of concentrations. Another important objective to highlight is to determine how the difference in the synthesis of these advanced adsorbent nanomaterials can condition their further behavior.

2. Experimental

2.1. Synthetic protocols

Synthesis of GO and assembly of CeO_2 NPs onto GO sheets

GO was prepared from bulk graphite (Alfa Aser) via the Hummers method [19]. Once the GO is successfully synthesized the strategies of *self-assembly* and *in-situ growth* are used as routes to obtain a hybrid nanomaterial constituted of CeO_2 NPs on rGO, obtaining then, the CeO_2/rGO nanomaterial.

Synthesis of 6-aminohexanoic acid CeO_2 NPs and their deposition onto GO by *self-assembly approach.*

The method to AHA-stabilized CeO_2 NPs can be found in the literature using some modifications [1]. Firstly, a solution containing 0.87 g of $Ce(NO_3)_3 \cdot 6H_2O$ and 80 ml of deionized water was heated to 95°C under magnetic stirring. Then, 8 ml aqueous solution with 1.05 g of

105 AHA and 40 µl of 37% HCl solution were added in sequence to the previous solution. The final
106 solution was kept at 95°C for 6 h. The resultant solution is a homogeneous suspension containing
107 positively charged CeO_2 NPs.

108 Subsequently, the assembly process was conducted by mixing the CeO_2-AHA NPs and GO
109 nanosheets, followed by a reduction process of the GO to rGO. To obtain the negatively charged
110 GO nanosheets a colloidal dispersion of 130 mg of graphite oxide and 433.33 mg of PVP were
111 dispersed in 345 ml of deionized water by sonication for about 30 min. Afterwards 43.33 ml of
112 positively charged CeO_2-AHA suspension was slowly added under magnetic stirring. After 4 h
113 of stirring, 2 ml (2 nM) of ascorbic acid was added to the above solution. The resulting mixture
114 was refluxed at 95°C for 1 h. The solid product was separated by centrifugation and well washed
115 with water and ethanol to remove any impurities and then dried at 50°C for 24 h. Finally, the
116 obtained product was designed as CeO_2/rGO-AHA.

117 Synthesis of acrylamide CeO_2 NPs and their deposition onto GO by self-assembly approach

118 The method followed to synthesize the CeO_2/rGO-AM was previously describe by Ling et al.
119 [16]. A solution of 1 mM $Ce(NO)_3 \cdot 6H_2O$ and 5 mM AM were dissolved in 26 ml N,N-
120 dimethylformamide (DMF) with ultrasonic treatment. At the same time, 130 mg of GO was
121 dispersed into 260 ml distilled water also with ultrasonic treatment for 2 h to form a brown
122 solution.

123 For the assembly, the above two solutions were mixed and heated to 90°C with continuous
124 stirring for 1 h. Then, 2 ml of ascorbic acid (2 mM) were added to reduce the GO and the
125 solutions were refluxed at 90°C for 6 h. The solid was separated by centrifugation and washed

several times with ethanol and distilled water before drying at 60°C for 24 h. The final product is designed as CeO_2/rGO-AM.

Synthesis of CeO_2 NPs with hexamethylenetetramine and their deposition onto GO by in-situ growth

The synthesis of CeO_2 NPs by using HMT was proceeded by an *in-situ* growth. The synthetic procedure was followed the conditions to precipitate the CeO_2 NPs reported by Zhang et al.[15] with the following modifications in order to achieve stabilization. A solution of 0.5 mM AM dissolved in 20 ml DMF with ultrasonic treatment is mixed with 0.04 M of $Ce(NO_3)_3 \cdot 6H_2O$ under stirring for 30 min. Then, a solution of HMT 0.5 M and 130 mg of GO, also with ultrasonic treatment, was added to the previous solution. After 1 h stirring 2 ml of 2 mM of ascorbic acid was added. The final solution was maintained under mild stirring and room temperature for 24 h. The product was washed several times with ethanol and water and dried at 60°C for 24 h. The nanocomposite material is designed as CeO_2/rGO-HMT.

2.2. Characterization methods

Raman spectrometry

Raman spectra were recorded using a Renishaw 1000 micro-Raman system fitted with a Leica microscope and the Grams Research™ analysis software. The excitation wavelength was 633 nm from a Renishaw RL633 HeNe laser. The 50x magnifying objective of the Leica microscope was capable of focusing the beam onto a spot of approximately 2–3 μm in diameter. Analysis performed at the Trinity College (Dublin).

Transmission electron microscopy

147 TEM images were obtained on a Jeol JEM-2100. Samples were prepared by deposition of each
148 of the CeO_2/rGO nanomaterials dispersed in water onto a carbon coated 300 mesh copper grid.
149 Diameters were measured with the Image J software program and the average values were
150 calculated by counting a minimum of 100 particles. Analysis performed in the CRANN
151 Advanced Microscopy Facility (AML) at Trinity College (Dublin).

152 Metal determination by Inductively Coupled Plasma-Optical Emission Spectrometry

153 The samples solutions containing heavy metal ions were acidified with concentrated HNO_3
154 (Merk p.a quality) until HNO_3 1% (p/v). The determination of the concentration of cadmium (II),
155 lead (II) and chromium (VI) was performed by Inductively Coupled Plasma-Optical Emission
156 Spectrometry, ICP-OES, Perkin-Elmer Optima 4300DV model. The experimental analysis was
157 performed by the *Servei d'Anàlisi Química* at the Autonomous University of Barcelona.

158 2.3. Metal adsorption experiments and isotherm models

159 The adsorption experiments were performed using cadmium (II) chloride (99.9%), lead (II)
160 nitrate (99.9%) and potassium dichromate (VI) (99.5%) as metal sources. To test the adsorption
161 capacity and determine the adsorption isotherms of the different nanomaterials synthesized in a
162 wide range of metal concentration, eight dilutions of cadmium, lead and chromium (5, 30 50,
163 100, 150, 200, and 250 mg/L) were carried out. Each of these solutions were mixed with 0.05 mg
164 of CeO_2/rGO (HMT, AM and AHA) nanomaterial. rGO was used as control at the same
165 conditions. All the experiments were stirred at 200 rpm at room temperature for 24 hours. No
166 adjustment in the pH was performed (pH= 5.5-6). The samples were filtrated (40 μm) to separate
167 the nanomaterial (solid phase) from the liquid phase. The supernatant was analyzed for residual

168 dissolved heavy metals (non-adsorbed metal). The adsorption capacity at the equilibrium was
169 calculated with the following equation [20]:

170 $$q=(C_0-C_e)V/m \qquad \text{(Eq.1)}$$

171 where C_0 and C_e are the initial and equilibrium concentrations of the heavy metal (mg/L)
172 respectively, V is the volume (L) and m (g) is the mass of the NPs.

173 Normally, the adsorption of metal ions from aqueous solutions is largely based on ion exchanges
174 or chemical/physical adsorptions on specific sites of the adsorbents, and therefore the pore
175 structures and surface areas of the adsorbents would play a crucial role [21]. Equilibrium
176 adsorption isotherms are typically used to determine the capacities of adsorbents. The most
177 common models used are the Langmuir, Temkin and the Freundlich models. Therefore, these
178 models were used to fit the experimental data [20]. The linear forms of the Langmuir, Temkin
179 and Freundlich models are listed in Table 1.

180 Table 1. Summary of equilibrium isotherms (K_L, K_F, K_T: Langmuir, Freundlich, Temkin
181 constants; n: heterogeneity coefficient; q_m: maximum adsorption capacity; q_e: adsorption
182 capacity at equilibrium; Ce: equilibrium concentration; b: activity coefficient related to mean
183 sorption energy).

Isotherm model	Equation
Langmuir	$C_e/q_e = 1/K_L q_m + C_e/q_m$
Freundlich	$\log q_e = \log K_F + 1/n \log C_e$
Temkin	$q_e = Rt/b \ln K_T + RT/b \ln C_e$

184

185 3. Results and discussion

3.1. Structural characterization of the nanomaterials

We have described two different strategies for the fabrication of CeO_2/rGO nanomaterials: *in situ* growth to obtain CeO_2/rGO-HMT and, the *self-assembly* approach to obtain CeO_2/rGO-AHA and CeO_2/rGO-AM. The synthetics protocols for obtaining the nanocomposites are described in the Figure 1.

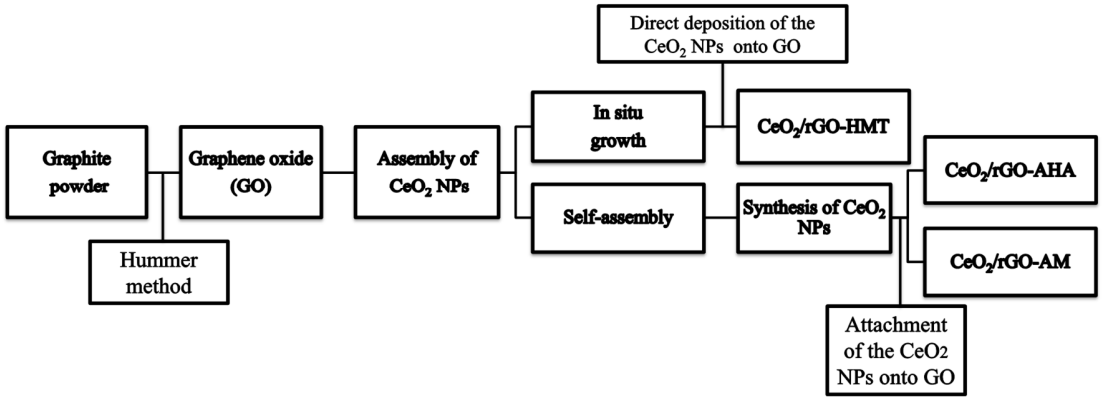

Figure 1. Synthesis of CeO_2/rGO nanocomposites by in situ growth and self-assembly method.

For the formation of CeO_2/RGO-AM nanomaterial, Ling et al. [16] proposed a similar *self-assembly* approach . Briefly, the AM is hydrolyzed to produce a polymer that reacts with the metal ions and forms a polymer metal complex (PMC), where the cerium ions and the amino groups are bonded. The PMC with a positive charge is attracted by the GO negatively charged and the self-assembly befalls once again by electrostatic attraction; therefore the metal ions are anchored to the surface of the GO maintaining the layered structure and finally reduced with ascorbic acid.

In the case of the *in-situ synthesis* the methodology proposed by Zhang et al. [15] to obtain CeO_2 NPs were used with some modifications. In this work, the AM is added in the first step (hydrolysis of the cerium salt) of the synthesis of CeO_2 NPs using HMT to form the PMC which generate a positive charge in the surface as well as favor the dispersion of the NPs on the surface of the GO, as shown in the above synthesis. The GO is directly mixed with the HMT and then added to the cerium solution in order that the hydroxyl ions oxidase the cerium and therefore obtain the NPs anchored on the surface of the GO [22].

Each product was characterized by Raman spectroscopy and Transmission Electron Microscopy.

3.2. Raman spectroscopy

Raman scattering is a powerful tool to characterize carbon based materials in a non-destructive way. The most prominent features in the Raman spectra of monolayer graphene are the so-called G band appearing at 1582 cm^{-1} (graphite) and the G′ band at about 2700 cm^{-1} using laser excitation at 2.41 eV. Figure 2 shows the Raman spectra of the CeO_2/rGO-AHA (by self-assembly), CeO_2/rGO-HMT (by in-situ) and the rGO. Two distinct peaks corresponding to the well-known G and D bands are displayed. The G band is usually assigned to the vibration of sp^2 carbon atoms in a graphitic 2D hexagonal lattice, while the D band is associated with the vibrations of sp^3 carbon atoms of defects and disorder [1,5]. In a typical synthesis, rGO showed D-band at 1345cm^{-1} and G-band at 1598cm^{-1}. After the reduction, the D-band remained the same but G-band shifted to lower frequency region (1580cm^{-1}), confirming the reduction [12]. The corresponding peak for CeO_2 NPs has been reported between 462 cm^{-1} and 467 cm^{-1} [16,23,24], however the peak at 455 cm^{-1} present in Figure 1is attributed to CeO_2 NPs and the shift associated to the successful attachment on the rGO in both cases. Furthermore, it is

observed a difference in the signal intensity for the peaks corresponding to both the CeO_2 NPs and the rGO, obtaining a NPs/rGO intensity ratio higher for the CeO_2/rGO-HMT (Figure 2b) than for CeO_2/rGO-AHA (Figure 2c). This result could suggest a higher concentration of CeO_2 NPs for the in-situ mechanism in the CeO_2/rGO-HMT nanocomposite.

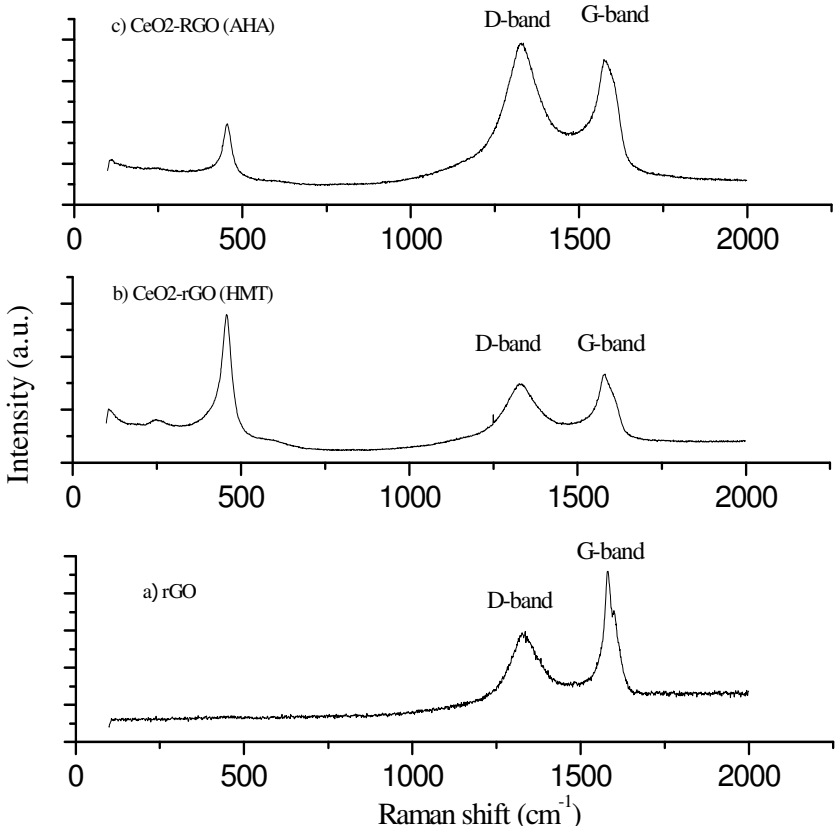

Figure 2. Ramman spectra of (a) rGO, (b) CeO_2/rGO-HMT by *in situ* and (c) CeO_2/rGO-AHA by *self-assembly.*

3.3. Transmission Electron Microscopy

TEM technique was used to elucidate the size, morphology and microstructure of the rGO-based nanomaterials, by dropping a small quantity of the dispersion onto holey carbon grids [25].

Figure 3 shows the TEM images of the CeO_2/rGO nanomaterials prepared by both strategies: *self-assembly,* CeO_2/rGO-AM and CeO_2/rGO-AHA and, *in situ* growth, CeO_2/rGO-HMT, as well as their size distribution.

As shown in Figure 3-A, CeO_2/rGO-AM are uniformly deposited and dispersed on the reduced graphene oxide. The size distribution of the CeO_2 –AM NPs falls in the range of 2.10±0.40 nm (Figure 2-A'). Figure 3-B showed CeO_2-AHA NPs deposited on the surface of the rGO with a distribution size of 16.12±2.24 nm (Figure 3-B'). Although the *self-assembly* approach involves two steps in order to obtain the nanocomposite, this feature allows a good control of the NPs size. The TEM image of the CeO_2/rGO-HMT (Figure 3-C) presents high density of CeO_2-NPs attached to the rGO with a NPs distribution size in the range of 3.343±0.701 nm (Figure 2-C'). The distribution size parameters are detailed in *Supplementary Information, S.I.2*. The higher concentration of the NPs, observed here, was also demonstrated with the previous discussed Raman results. The *in situ* synthesis possesses the advantage of fabricate the nanomaterial in one step, however the size, the morphology and the distribution of the nanoparticles cannot be well controlled due to many factors, such as defects in the surface of the GO sheet, the temperature, etc [13].

Figure 3. TEM images of (A) CeO_2/rGO-AM, (B) CeO_2/rGO-AHA and (C) CeO_2/rGO-HMT nanocomposites as well as the size distribution (A', B' and C').

3.4. Adsorption Isotherms

The adsorption of lead (II), cadmium (II) and chromium (VI) from aqueous solutions onto rGO nanosheets impregnated with CeO_2-NPs were tested, synthetized by the different mentioned protocols.

Respectively, Tables 2 and 3 show the adsorption capacities of lead (II) and cadmium (II) with each adsorbent here reported, as well as the final metal concentration. It was observed that mainly lead (II) showed changes in the concentration (Table 2), while cadmium (II) was adsorbed at lower concentrations (Table 3). Moreover, the adsorption of chromium (VI) in solution does not follow a clear tendency and therefore, no adsorption model could be applied. The adsorption experiments for the removal of Cr (VI) are shown in *S.I.3*. It is worthwhile to mention that although chromium is dissolved as hexavalent chromium, chromium is actually present in its anionic form thus, the repulsion with the negative charge of the rGO appear to be stronger than the interaction with the NPs showing very little affinity for the nanomaterial.

The highest adsorption capacity was obtained for the CeO_2/rGO-HMT material (95.75 mg Pb^{2+}/g CeO_2/rGO-HMT), almost the double than that obtained with the rGO (49.927 mg Pb^{2+}/g rGO) and significantly higher than the other self-assembly synthetized nanomaterials (46.78 mg Pb^{2+}/g CeO_2/rGO-AHA and 62.80 mg Pb^{2+}/g CeO_2/rGO-AM). This may be attributed to the fact that the actual CeO_2-NPs concentration of the CeO_2/rGO-HMT composite is higher than in the others, as demonstrated by both, Raman and TEM techniques. The small size of the CeO_2 NPs, as well as the concentration, may also offered higher surface area for the adsorption of the lead (II). Obtained adsorption capacity is in the middle range of reported literature values. While non-nanomaterials showed lower adsorption capacities such as *Ficus religiosa* leaves (37.45 mg Pb^{2+}/g) [26], plant maize (2.3 mg Pb^{2+}/g) [27] or bagasse fly ash, (2.50 mg Pb^{2+}/g) [28]; some metal oxide NPs (181.2 mg Pb^{2+}/g CeO_2 and 153.24 mg Pb^{2+}/g TiO_2) [3] showed higher adsorption capacities than the rGO-based nanocomposites here presented.

Table 2. Adsorption experiments for the removal of Pb (II) dissolved in water with different CeO_2/rGO nanomaterials.

Initial Pb (II) concentration	Adsorption capacities and final metal concentrations							
	rGO		CeO_2/rGO-AHA		CeO_2/rGO-AM		CeO_2/rGO-HMT	
Ci (mg/L)	C_e (mg/L)	q_t (mg/g)	C_e (mg/L)	q_t (mg/g)	C_e (mg/L)	q_t (mg/g)	C_e (mg/L)	q_t (mg/g)
5	0.50	18.00	0.73	17.10	0.59	17.62	0.50	18.00
10	2.04	31.85	2.95	28.21	3.99	24.02	2.37	30.53
30	22.56	29.77	19.84	40.65	22.50	29.98	16.29	54.85
50	40.85	36.58	38.04	47.85	42.78	28.89	30.95	76.19
100	87.52	49.93	85.55	57.80	91.43	34.28	77.54	89.84
150	*	N/A	137.92	48.32	141.55	33.79	132.56	69.77
200	196.02	15.90	187.08	51.70	186.36	54.54	182.86	68.56
250	*	N/A	238.30	46.78	234.30	62.80	226.06	95.76

C_e is the concentration of the metal ions at equilibrium; q_t is the adsorption capacity measured after 24 h and expressed in mg metal / g nanomaterial; *Higher than the initial concentration; N/A: not available

From the adsorption capacity values for the removal of cadmium (Table 3), it can be observed that the maximum value was obtained with the CeO_2/rGO-AM being 31.26 mg Cd^{2+}/ g CeO_2/rGO-AM which is double than the one corresponding to rGO (15.42 mg Cd^{2+}/g rGO). It can be seen that the values obtained with GO are similar to the ones obtained with CeO_2/rGO-HMT (11.67 mg Cd^{2+}/g CeO_2/rGO-HMT) and CeO_2/rGO-AHA (16.71 mg Cd^{2+}/g CeO_2/rGO-AHA) which can be compared with those obtained with Filtrasorb 400 (9.5 mg Cd^{2+}/g) [29], carbon aerogel (15.5 Cd^{2+}/g) [30], Indonesian peat (14 mg Cd^{2+}/g) [31] or TiO_2 (15.83mg Cd^{2+}/g TiO_2) [2] while Fe_3O_4 (99.57 mg Cd^{2+}/g Fe_3O_4) [2] and CeO_2 (48.30 mg Cd^{2+}/g CeO_2) [2] presented higher adsorption capacities. Even though CeO_2 NPs by themselves showed higher

adsorption capacity for Cd^{2+} than the materials here reported, it is worthy that the CeO_2 based nanosheets present other advantages including NPs stability. Pb(II) ions showed higher removal percentages than Cd(II) ions which it is in agreement with the metal electronegativity associated to each metal. The tables of the percent removal for Pb(II) and Cd (II) are sown in *S.I.4* and *S.I.5*, respectably.

Table 3. Adsorption experiments for the removal of Cd (II) dissolved in water with different CeO_2/rGO nanomaterials.

Initial Cd(II) concentration	Adsorption capacities and final metal concentrations							
	rGO		CeO_2/rGO-AHA		CeO_2/rGO-AM		CeO_2/rGO-HMT	
C_i (mg/L)	C_e (mg/L)	q_t (mg/g)	C_e (mg/L)	q_t (mg/g)	C_e (mg/L)	q_t (mg/g)	C_e (mg/L)	q_t (mg/g)
5	2.47	10.11	4.49	2.03	2.82	8.71	3.32	6.72
10	6.14	15.43	9.20	3.19	7.77	8.92	7.08	11.67
30	27.24	11.03	30.58	N/A	28.85	4.58	27.10	11.57
50	49.00	4.00	45.82	16.71	49.08	3.69	50.01	N/A
100	*	N/A	*	N/A	99.47	2.12	*	N/A
150	*	N/A	*	N/A	*	N/A	*	N/A
200	*	N/A	*	N/A	196.73	13.08	*	N/A
250	*	N/A	*	N/A	242.18	31.26	*	N/A

*Higher than the initial concentration; C_e: concentration of the metal ions at equilibrium; q_t: adsorption capacity measured after 24 h and expressed in mg metal / g nanomaterial; N/A: not available

The electronegativity can be treated as one of the contributing parameters to the metal ion uptake because in the case of adsorption of metal cations on a negatively charged surface plays a

302 significant role in the adsorption process, being the electronegativity of Pd^{2+} higher than Cd^{2+}
303 [32].

304 These results can be attributed not only to the high surface area due to the presence of the CeO_2
305 NPs and its composition, but also to the high oxygen content of GO [17]. In addition, the
306 abundant oxygen-containing functional groups on the surfaces of GO nanosheets make the
307 adjacent oxygen atoms available to bind metal ions [33].

308 The optimization of an adsorption process requires an understanding of the driving forces that
309 govern the interaction between adsorbate and the adsorbent, therefore it is important to establish
310 the most appropriate correlation for the equilibrium.[34,35]. The data obtained for the removal of
311 cadmium (II) and lead (II) in adsorption were fitted to the Freundlich, Langmuir and Temkin
312 isotherm models. The sorption behavior for each metal ion onto the different nanomaterials is
313 shown in Figure 3 and 4. The parameters of each adsorption model were calculated and listed in
314 the Table 4. Only the available data obtained from the adsorption experiments was used in the
315 fitting of the adsorption models. The regression coefficient (R^2) show that the Langmuir model
316 fitted better than the Freundlich and the Temkin models, suggesting that Pb(II) ions adsorption
317 on the three different nanocomposites and the rGO are all monolayer coverage. The Langmuir
318 isotherm best describes chemisorption processes. Chemisorption involves a more specific
319 binding of the adsorbate to the solid, in this case of the heavy metal ion to the CeO_2/rGO
320 nanocomposite. It is a process that is more similar to a chemical reaction, involving valence
321 forces through sharing or the exchange of electrons between sorbent and sorbate and hence, only
322 monolayer adsorption is possible (i.e. oxygen atoms binding with metal ions) [36]. Sitko et al.
323 [32] investigated the XPS spectra for GO with adsorbed divalent metal ions, among them Cd(II)
324 and Pb(II), and observed a significant difference between oxygen peaks suggesting that the

325 nature of the adsorption of the metal ions on GO is chemical, in accordance with the process
326 described by the Langmuir model. In addition, the point of zero charge (pHpzc) value of GO is
327 3.8–3.9. Therefore, at pH > 3.9, the surface charge of GO is negative and the electrostatic
328 interactions between the metal ions and GO nanosheets become stronger [33,37–39]. On the
329 other hand Cao et al. [40] synthesized ceria hollow nanospheres composed of CeO_2 nanocrystals
330 and used as adsorbent for the removal of As (V), Cr(VI) and Pb(II). They suggest that the
331 adsorption mechanisms of the heavy metals ions on the metal oxide are likely the combination of
332 static electrical attraction between oxides and heavy metal ions and ion exchange. The Temkin
333 isotherm contains a factor (*b*) that explicitly takes into account adsorbent–adsorbate interactions.
334 By ignoring the extremely low and large value of concentrations, the model assumes that heat of
335 adsorption (function of temperature) of all molecules in the layer would decrease linearly rather
336 than logarithmic with coverage [41,42]. On the other hand, the Freundlich coefficient (*n*), which
337 should have values ranging from 1 to 10 and in this case is high (5.28–6.76), supports the
338 favorable adsorption of the lead ions onto the adsorbent [43]. Moreover, in Table 4 it is possible
339 to observe that the data obtained for the removal of cadmium (II) with rGO did not fit the linear
340 models (negative coefficients), leading to the conclusion that the adsorption behavior of the
341 tested systems was very difficult. However, good R^2 values for Langmuir and Freundlich models
342 were obtained with CeO_2/rGO-HMT and CeO_2/rGO-AHA.

343

344

345 Table 4. Parameters for Langmuir, Freundlich and Temkin models of Pb(II) and Cd(II) ions
346 adsorption on different CeO_2/rGO nanomaterials and rGO as reference sample.

		Lead			Cadmium		
		Parameter			Parameter		
Isotherm	Adsorbent	q_m (mg/g)	K_L (L/mg)	R^2	q_m (mg/g)	K_L (L/mg)	R^2
Langmuir	rGO	50.25	0.15	0.9066	4.024	-0.17	0.8797
	CeO_2/rGO-HMT	83.33	0.07	0.9477	12.39	0.58	0.9913
	CeO_2/rGO-AHA	48.78	0.52	0.9937	156.25	0.003	0.1694
	CeO_2/rGO-AM	63.69	0.04	0.9145	14.12	0.05	0.9212
		K_F	n	R^2	K_F	n	R^2
Freundlich	rGO	22.46	6.68	0.7673	17.85	-3.68	0.4111
	CeO_2/rGO-HMT	23.86	4.05	0.9238	3.29	1.86	0.879
	CeO_2/rGO-AHA	20.89	5.05	0.9119	0.46	1.08	0.9900
	CeO_2/rGO-AM	17.77	5.28	0.8538	6.33	4.64	0.6627
		K_T	b	R^2	K_T	B	R^2
Temkin	rGO	126.97	4.56	0.7314	0.001	-2.04	0.6481
	CeO_2/rGO-HMT	5.44	13.87	0.9674	0.28	14.80	0.8043
	CeO_2/rGO-AHA	31.50	6.11	0.9603	0.24	6.68	0.9459
	CeO_2/rGO-AM	664.54	3.00	0.6955	2.67	3.48	0.5405

347

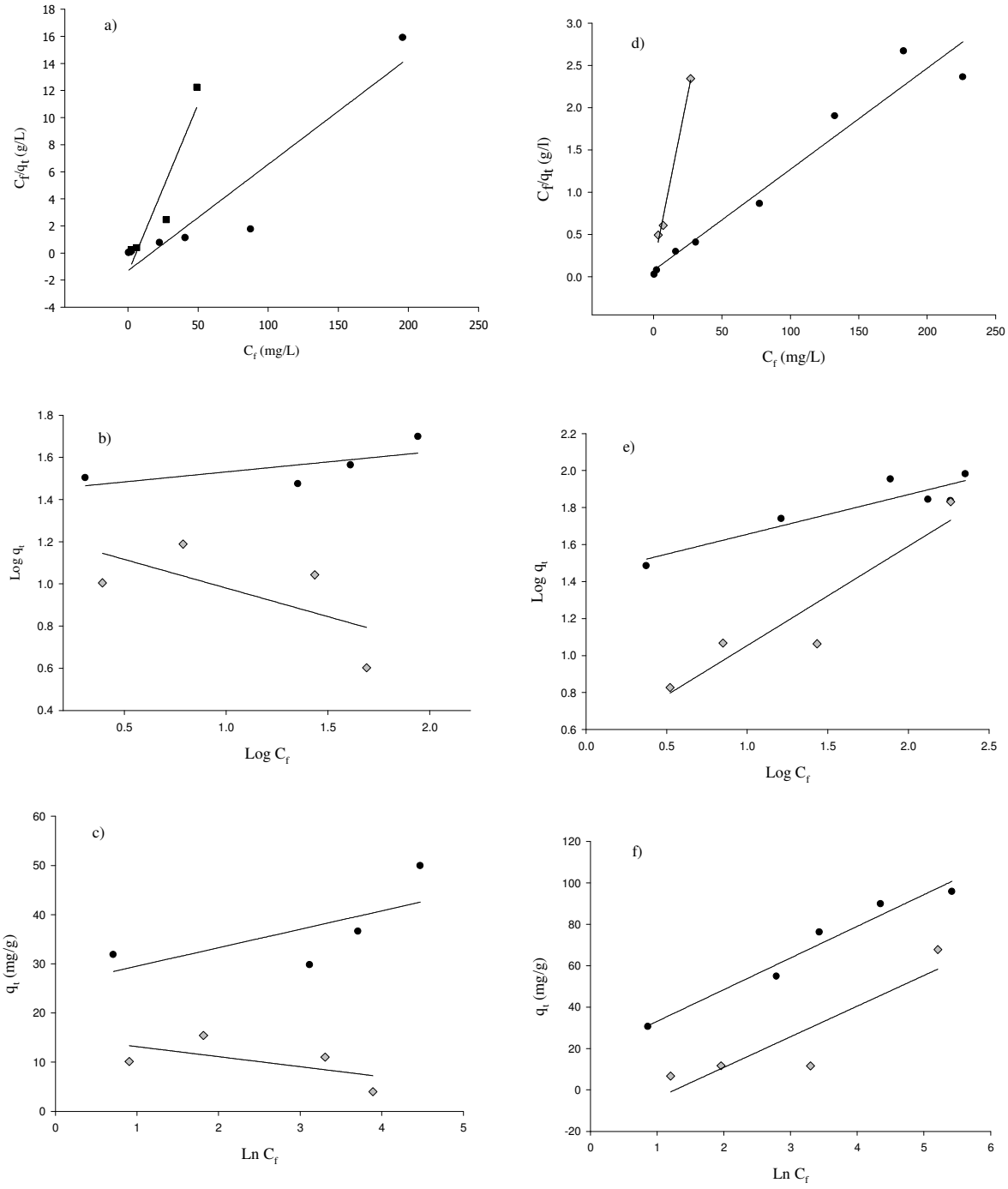

Figure. 3 a) Langmuir isotherm , b) Freundlich isotherm, c) Temkin isotherm for the adsorption of Pb(II) (circle) and Cd (II) (diamond) onto rGO; d) Langmuir isotherm, e) Freundlich isotherm, f) Temkin isotherm for the adsorption of Pb(II) (circle) and Cd (II) (diamond) onto CeO_2/rGO-HTM.

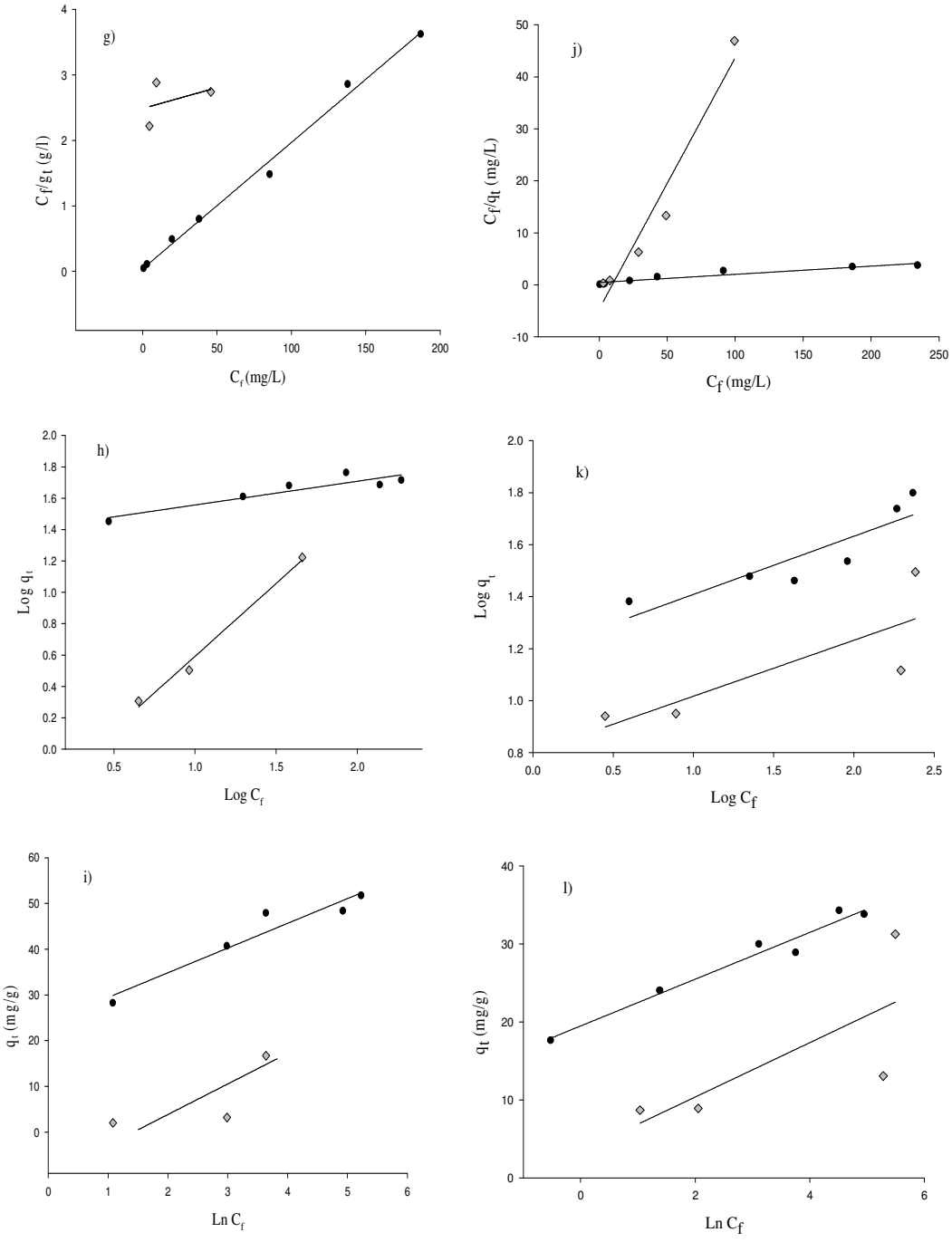

353

354 Figure. 4. g) Langmuir isotherm , h) Freundlich isotherm, i) Temkin isotherm for the adsorption
355 of Pb(II) (circle) and Cd (II) (diamond) onto CeO_2/rGO-AHA; j) Langmuir isotherm, k)
356 Freundlich isotherm, l) Temkin isotherm for the adsorption of Pb(II) (circle) and Cd (II)
357 (diamond) onto CeO_2/rGO-AM.

Overall, the *self-assembly* approach produced nanomaterials with CeO_2 NPs with controlled size on rGO sheets. This is a key step in the process for the preparation of well-defined NPs to position itself as an advantageous synthetic procedure [1]. However, the material synthesized by *in-situ* growth, simplify the process avoiding a prior step of the preparation of the CeO_2 NPs.

The adsorption results suggest that the new CeO_2-rGO nanocomposites synthesized by two different procedures presented promising results for adsorption of cationic water contaminants. The adsorption mechanism has contribution from both the negative functional groups of the rGO and the surface of the CeO_2-NPs.

Moreover, these reported methods offer potentially low cost and large scale production of graphene-based hybrid materials suitable for water purification [44]. This is due to the inorganic nanoparticles present in 2D graphene nanocomposites prevent graphene aggregation, as such a high surface area and pore volume can be maintained [14].

4. Conclusions

Graphene oxide as well as the CeO_2/rGO nanocomposites was successfully synthesized. The Raman spectroscopy showed the peak associated to the G (1580 cm^{-1}) and D (1345 cm^{-1}) bands of the rGO and the peak of the CeO_2 NPs at 455cm^{-1}, which confirms that cerium oxide nanoparticles were anchored to the surface. The size of the CeO_2 NPs attached to GO, was from 2 nm to 16 nm (depending on the synthesis pathway). The highest percentage removal (90%) was obtained with CeO2/rGO-HMT for the removal of Pb (II). The R^2 for Langmuir (0.907-0.994) isotherm model suggests chemisorption and monolayer coverage. Although Pb (II) and Cd (II) showed the main adsorption capacities, Cr (VI) was removed at lower concentrations. Future studies will explore the recycling of

the nanomaterial to give a better understanding of the reusability of the adsorbent. Another important parameter is to test the nanomaterial in multicomponent systems as a first step towards their use with real wastewaters.

Supporting Information. Size distribution parameters as Supporting Information is included.

ACKNOWLEDGMENT

A.R. Contreras Rodríguez thanks the financial support through the scholarship provided by the Consejo Nacional de Ciencia y Tecnología (CONACYT, México).

REFERENCES

[1] Z. Ji, X. Shen, M. Li, H. Zhou, G. Zhu, K. Chen, Synthesis of reduced graphene oxide/CeO2 nanocomposites and their photocatalytic properties, Nanotechnology. 24 (2013) 1–9.

[2] A.R. Contreras, A. García, E. González, E. Casals, V. Puntes, A. Sánchez, et al., Potential use of CeO2 , TiO2 and Fe3O4 nanoparticles for the removal of cadmium from water, Desalin. Water Treat. 41 (2012) 296–300.

[3] S. Recillas, A. García, E. González, E. Casals, V. Puntes, A. Sánchez, et al., Use of CeO2, TiO2 and Fe3O4 nanoparticles for the removal of lead from water. Toxicity of nanoparticles and derived compounds, Desalination. 277 (2011) 213–220.

[4] S. Recillas, J. Colón, E. Casals, E. González, V. Puntes, A. Sánchez, et al., Chromium VI

401 adsorption on cerium oxide nanoparticles and morphology changes during the process., J.
402 Hazard. Mater. 184 (2010) 425–31.

403 [5] S. Wu, K. Zhang, X. Wang, Y. Jia, B. Sun, T. Luo, et al., Enhanced adsorption of
404 cadmium ions by 3D sulfonated reduced graphene oxide, Chem. Eng. J. 262 (2015) 1292–
405 1302.

406 [6] S. Wang, H. Sun, H.M.M. Ang, M.O.O. Tadé, Adsorptive remediation of environmental
407 pollutants using novel graphene-based nanomaterials, Chem. Eng. J. 226 (2013) 336–347.

408 [7] K. Lü, G.X. Zhao, X.K. Wang, A brief review of graphene-based material synthesis and
409 its application in environmental pollution management, Chinese Sci. Bull. 57 (2012)
410 1223–1234.

411 [8] R.L. White, C.M. White, H. Turgut, A. Massoud, Z.R. Tian, Comparative studies on
412 copper adsorption by graphene oxide and functionalized graphene oxide nanoparticles, J.
413 Taiwan Inst. Chem. Eng. 0 (2018) 1–11.

414 [9] Y. Wen, H. Ding, Y. Shan, Preparation and visible light photocatalytic activity of
415 Ag/TiO2/graphene nanocomposite, Nanoscale. 3 (2011) 4411–4417.

416 [10] K. Singh, A. Ohlan, V.H. Pham, B. R, S. Varshney, J. Jang, et al., Nanostructured
417 graphene/Fe_3O_4 incorporated polyaniline as a high performance shield against
418 electromagnetic pollution., Nanoscale. 5 (2013) 2411–2420.

419 [11] A.E. Burakov, E. V. Galunin, I. V. Burakova, A.E. Kucherova, S. Agarwal, A.G.
420 Tkachev, et al., Adsorption of heavy metals on conventional and nanostructured materials

421 for wastewater treatment purposes: A review, Ecotoxicol. Environ. Saf. 148 (2018) 702–
422 712.

423 [12] T.S. Sreeprasad, S.M. Maliyekkal, K.P. Lisha, T. Pradeep, Reduced graphene oxide-
424 metal/metal oxide composites: facile synthesis and application in water purification., J.
425 Hazard. Mater. 186 (2011) 921–31.

426 [13] H. Wang, X. Yuan, Y. Wu, H. Huang, X. Peng, G. Zeng, et al., Graphene-based materials:
427 fabrication, characterization and application for the decontamination of wastewater and
428 wastegas and hydrogen storage/generation., Adv. Colloid Interface Sci. 195–196 (2013)
429 19–40.

430 [14] K.C. Kemp, H. Seema, M. Saleh, N.H. Le, K. Mahesh, V. Chandra, et al., Environmental
431 applications using graphene composites: water remediation and gas adsorption,
432 Nanoscale. 5 (2013) 3149–3171.

433 [15] F. Zhang, Ceria nanoparticles: Size, size distribution, and shape, J. Appl. Phys. 95 (2004)
434 4319–4326.

435 [16] Q. Ling, M. Yang, R. Rao, H. Yang, Q. Zhang, H. Liu, et al., Simple synthesis of layered
436 CeO2–graphene hybrid and their superior catalytic performance in dehydrogenation of
437 ethylbenzene, Appl. Surf. Sci. 274 (2013) 131–137.

438 [17] R. Sitko, B. Zawisza, E. Malicka, Graphene as a new sorbent in analytical chemistry,
439 TrAC Trends Anal. Chem. 51 (2013) 33–43.

440 [18] T. Yu, J. Zeng, B. Lim, Y. Xia, Aqueous-phase synthesis of Pt/CeO2 hybrid

nanostructures and their catalytic properties, Adv. Mater. 22 (2010) 5188–5192.

[19] J.W.S. Hummers, R.E. Offeman, Preparation of Graphitic Oxide, J. Am. Chem. Soc. 80 (1958) 1339. doi:10.1021/ja01539a017.

[20] H.K. Boparai, M. Joseph, D.M. O'Carroll, Kinetics and thermodynamics of cadmium ion removal by adsorption onto nano zerovalent iron particles., J. Hazard. Mater. 186 (2011) 458–465.

[21] J.-G. Yu, L.-Y. Yu, H. Yang, Q. Liu, X.-H. Chen, X.-Y. Jiang, et al., Graphene nanosheets as novel adsorbents in adsorption, preconcentration and removal of gases, organic compounds and metal ions., Sci. Total Environ. 502 (2015) 70–79.

[22] A.R. Contreras Rodrírgez, A. Sánchez, X. Font, Removal of cadmium (II), lead (II) and chromium (VI) in water with nanomaterials, Universitat Autònoma de Barcelona, 2015.

[23] F. Zhang, S.-W.W. Chan, J.E. Spanier, E. Apak, Q. Jin, R.D. Robinson, et al., Cerium oxide nanoparticles: Size-selective formation and structure analysis, Appl. Phys. Lett. 80 (2002) 127.

[24] B. Sabu, T. Varghese, Structural characterization and optical studies of CeO 2 nanoparticles synthesized by chemical precipitation, Indian J. Pure Appl. Phys. 53 (2015) 596–603.

[25] Y. Hernandez, V. Nicolosi, M. Lotya, F.M. Blighe, Z. Sun, S. De, et al., High-yield production of graphene by liquid-phase exfoliation of graphite., Nat. Nanotechnol. 3 (2008) 563–568.

461 [26] S. Qaiser, A.R. Saleemi, M. Umar, Biosorption of lead from aqueous solution by Ficus
462 religiosa leaves: batch and column study., J. Hazard. Mater. 166 (2009) 998–1005.

463 [27] Y. Zhang, C. Banks, A comparison of the properties of polyurethane immobilised
464 Sphagnum moss, seaweed, sunflower waste and maize for the biosorption of Cu, Pb, Zn
465 and Ni in continuous flow packed columns., Water Res. 40 (2006) 788–98.

466 [28] V.K. Gupta, I. Ali, Removal of lead and chromium from wastewater using bagasse fly
467 ash--a sugar industry waste., J. Colloid Interface Sci. 271 (2004) 321–8.

468 [29] M. Sánchez-Polo, J. Rivera-Utrilla, Adsorbent-adsorbate interactions in the adsorption of
469 Cd(II) and Hg(II) on ozonized activated carbons, Environ. Sci. Technol. 36 (2002) 3850–
470 3854.

471 [30] J. Goel, K. Kadirvelu, C. Rajagopal, V.K. Garg, Cadmium (II) Uptake from Aqueous
472 Solution by Adsorption on Carbon Aerogel Using a Response Surface Methodological
473 Approach, Ind. Eng. Chem. Res. 45 (2006) 6531–6537.

474 [31] R. Balasubramanian, S. V. Perumal, K. Vijayaraghavan, Equilibrium isotherm studies for
475 the multicomponent adsorption of lead, zinc and cadmium onto Indonesian peat, Ind. Eng.
476 Chem. Res. 48 (2009) 2093–2099. doi:10.1021/ie801022p.

477 [32] R. Sitko, E. Turek, B. Zawisza, E. Malicka, E. Talik, J. Heimann, et al., Adsorption of
478 divalent metal ions from aqueous solutions using graphene oxide, Dalton Trans. 42 (2013)
479 5682–5689.

480 [33] G. Zhao, J. Li, X. Ren, C. Chen, X. Wang, Few-layered graphene oxide nanosheets for

heavy metal ion pollution management, Environ. Sci. Technol. 45 (2011) 1–4. doi:dx.doi.org/10.1021/es203439v.

[34] A. Rashid, H.N. Bhatti, M. Iqbal, S. Noreen, Fungal biomass composite with bentonite efficiency for nickel and zinc adsorption: A mechanistic study, Ecol. Eng. 91 (2016) 459–471.

[35] M. Mushtaq, H.N. Bhatti, M. Iqbal, S. Noreen, Eriobotrya japonica seed biocomposite efficiency for copper adsorption: Isotherms, kinetics, thermodynamic and desorption studies, J. Environ. Manage. 176 (2016) 21–33. doi:10.1016/j.jenvman.2016.03.013.

[36] R.J. Sime, The Langmuir Adsorption Isotherm, 2000.

[37] J. Wang, B. Chen, Adsorption and coadsorption of organic pollutants and a heavy metal by graphene oxide and reduced graphene materials, Chem. Eng. J. 281 (2015) 379–388.

[38] Y. Sun, Q. Wang, C. Chen, X. Tan, X. Wang, Interaction between Eu(III) and graphene oxide nanosheets investigated by batch and extended X-ray absorption fine structure spectroscopy and by modeling techniques, Environ. Sci. Technol. 46 (2012) 6020–6027.

[39] G. Zhao, T. Wen, X. Yang, S. Yang, J. Liao, J. Hu, et al., Preconcentration of U(vi) ions on few-layered graphene oxide nanosheets from aqueous solutions, Dalt. Trans. 41 (2012) 6182–6188.

[40] C.Y. Cao, Z.M. Cui, C.Q. Chen, W.G. Song, W. Cai, Ceria hollow nanospheres produced by a template-free microwave-assisted hydrothermal method for heavy metal ion removal and catalysis, J. Phys. Chem. C. 114 (2010) 9865–9870.

501 [41] K.Y. Foo, B.H. Hameed, Insights into the modeling of adsorption isotherm systems,
502 Chem. Eng. J. 156 (2010) 2–10.

503 [42] B.H. Hameed, I.A.W. Tan, A.L. Ahmad, Adsorption isotherm, kinetic modeling and
504 mechanism of 2,4,6-trichlorophenol on coconut husk-based activated carbon, Chem. Eng.
505 J. 144 (2008) 235–244.

506 [43] G. Alagumuthu, V. Veeraputhiran, R. Venkataraman, Adsorption Isotherms on Fluoride
507 Removal : Batch Techniques, Arch. Appl. Sci. Res. 2 (2010) 170–185.

508 [44] V. Chandra, J. Park, Y. Chun, J.W. Lee, I.C. Hwang, K.S. Kim, Water-dispersible
509 magnetite-reduced graphene oxide composites for arsenic removal, ACS Nano. 4 (2010)
510 3979–3986.

511